Targeting CYP2J to reduce paclitaxel-induced peripheral neuropathic pain

Marco Sisignano[a,1], Carlo Angioni[a], Chul-Kyu Park[b,c,2], Sascha Meyer Dos Santos[d], Holger Jordan[d], Maria Kuzikov[e], Di Liu[b,c], Sebastian Zinn[a], Stephan W. Hohman[a], Yannick Schreiber[a], Béla Zimmer[a], Mike Schmidt[d], Ruirui Lu[a,3], Jing Suo[a], Dong-Dong Zhang[a], Stephan M. G. Schäfer[a], Martine Hofmann[d], Ajay S. Yekkirala[f], Natasja de Bruin[d], Michael J. Parnham[d], Clifford J. Woolf[f], Ru-Rong Ji[b,c,g], Klaus Scholich[a], and Gerd Geisslinger[a,d]

[a]Institute of Clinical Pharmacology, Pharmazentrum Frankfurt/ZAFES (Zentrum für Arzneimittelforschung, Entwicklung und Sicherheit), University Hospital, Goethe-University, D-60590 Frankfurt, Germany; [b]Department of Anesthesiology, Duke University Medical Center, Durham, NC 27710; [c]Department of Neurobiology, Duke University Medical Center, Durham, NC 27710; [d]Fraunhofer Institute for Molecular Biology and Applied Ecology–Project Group Translational Medicine and Pharmacology (IME-TMP), D-60596 Frankfurt, Germany; [e]Fraunhofer Institute for Molecular Biology and Applied Ecology–ScreeningPort, D-22525 Hamburg, Germany; [f]F. M. Kirby Neurobiology Center, Department of Neurobiology, Harvard Medical School, Children's Hospital Boston, Boston, MA 02115; and [g]Pain Research Center, Brigham and Women's Hospital and Harvard Medical School, Boston, MA 02115

Edited by David Julius, University of California, San Francisco, CA, and approved September 14, 2016 (received for review August 17, 2016)

Chemotherapy-induced peripheral neuropathic pain (CIPNP) is a severe dose- and therapy-limiting side effect of widely used cytostatics that is particularly difficult to treat. Here, we report increased expression of the cytochrome-P_{450}-epoxygenase CYP2J6 and increased concentrations of its linoleic acid metabolite 9,10-EpOME (9,10-epoxy-12Z-octadecenoic acid) in dorsal root ganglia (DRGs) of paclitaxel-treated mice as a model of CIPNP. The lipid sensitizes TRPV1 ion channels in primary sensory neurons and causes increased frequency of spontaneous excitatory postsynaptic currents in spinal cord nociceptive neurons, increased CGRP release from sciatic nerves and DRGs, and a reduction in mechanical and thermal pain hypersensitivity. In a drug repurposing screen targeting CYP2J2, the human ortholog of murine CYP2J6, we identified telmisartan, a widely used angiotensin II receptor antagonist, as a potent inhibitor. In a translational approach, administration of telmisartan reduces EpOME concentrations in DRGs and in plasma and reverses mechanical hypersensitivity in paclitaxel-treated mice. We therefore suggest inhibition of CYP2J isoforms with telmisartan as a treatment option for paclitaxel-induced neuropathic pain.

chemotherapy-induced neuropathy | neuropathic pain | TRPV1 | telmisartan | oxidized lipids

Recent studies identified members of the transient receptor potential-family of ion channels (TRPV1, TRPA1, and TRPV4) as contributors to both mechanical and cold allodynia during oxaliplatin and paclitaxel-induced neuropathy (1–5). Activation or sensitization of TRPV1 and TRPA1 can lead to enhanced release of CGRP and substance P, both of which can cause neurogenic inflammation and recruitment of T cells (6, 7).

However, it remains unclear which endogenous mediators are involved in paclitaxel-dependent activation or sensitization of TRP channels, as paclitaxel cannot directly activate TRP channels (4, 5, 8). Interestingly, paclitaxel is an inducer of some Cytochrome-P_{450} epoxygenases (e.g., CYP2C8, CYP2C9) (9). CYP epoxygenases can metabolize ω-6 fatty acids, such as arachidonic acid (AA) and linoleic acid (LA), generating either lipid epoxides such as EETs (epoxyeicosatrienoid acids) or ω-hydroxides such as 20-hydroxyeicosatetraenoic acid (20-HETE) (10, 11).

Although therapeutic alternatives exist, paclitaxel is still the preferred first line of therapy for metastatic breast cancer (12), causing severe CIPNP in many treated patients. Here, we performed liquid chromatography–tandem mass spectrometry (LC–MS/MS)-based lipid profiling of sciatic nerve, dorsal root ganglion (DRG), and dorsal horn tissue from paclitaxel-treated mice.

We identified 9,10-EpOME (9,10-epoxy-12Z-octadecenoic acid), a CYP metabolite of LA, to be strongly synthesized in DRGs 24 h and 8 d after paclitaxel injection in mice. 9,10-EpOME is capable of sensitizing TRPV1 at submicromolar concentrations via a cAMP–PKA-dependent mechanism, causing enhanced frequency of spontaneous excitatory postsynaptic currents (sEPSCs) in lamina II neurons of the spinal cord, and sensitizes the release of TRPV1-dependent CGRP from isolated sciatic nerves and DRG cultures. Moreover, intrathecal and intraplantar injection of 9,10-EpOME causes a reduction of the mechanical thresholds of wild-type mice. We find a strong up-regulation of CYP2J6, the murine ortholog of human CYP2J2, in DRGs 8 d after paclitaxel injection that correlates with the EpOME levels. In a substance screen containing more than 600 approved substances, we identified different compounds that block CYP2J6 and human CYP2J2 and cause amelioration of paclitaxel-induced CIPNP in mice.

Results

Lipid Synthesis and CYP Expression During Paclitaxel-Induced Neuropathic Pain. To investigate paclitaxel-induced neuropathic pain (PIPN), we used a high dose (HD, 1×6 mg·kg^{-1}) and a multiple low-dose model (MLD, 4×2 mg·kg^{-1}) (2, 13). We monitored the mechanical thresholds of paclitaxel-treated animals and observed a strong mechanical hypersensitivity in paclitaxel-treated mice (Fig. 1 *A* and *B*) that did not differ between

Significance

Chemotherapy-induced peripheral neuropathic pain (CIPNP) is a severe side effect that affects up to 80% of patients during cancer treatment. Pharmacological treatment options are poor, as CIPNP differs mechanistically from other chronic pain states. Here, we describe a mechanism by which pronociceptive oxidized lipid mediators are generated by the cytochrome P_{450}-epoxygenase CYP2J2 in sensory neurons during CIPNP. Blocking the synthesis of these oxidized lipids with telmisartan, which we identified as a potent CYP2J2 inhibitor in a large drug repurposing screen, caused a robust reduction of paclitaxel-induced pain in mice in vivo. We therefore consider targeting CYP2J2 with telmisartan as a treatment option for chemotherapy-induced peripheral neuropathic pain in patients.

Author contributions: M. Sisignano, S.M.D.S., M.K., D.L., M.H., N.d.B., C.J.W., R.-R.J., K.S., and G.G. designed research; M. Sisignano, C.A., C.-K.P., S.M.D.S., H.J., M.K., D.L., S.Z., S.W.H., Y.S., B.Z., M. Schmidt, R.L., J.S., D.-D.Z., S.M.G.S., M.H., A.S.Y., N.d.B., and M.J.P. performed research; M. Sisignano, C.A., C.-K.P., S.M.D.S., H.J., M.K., D.L., Y.S., B.Z., R.L., M.H., A.S.Y., and K.S. analyzed data; and M. Sisignano, C.J.W., R.-R.J., K.S., and G.G. wrote the paper.

The authors declare no conflict of interest.

This article is a PNAS Direct Submission.

[1]To whom correspondence should be addressed. Email: Marco.Sisignano@med.uni-frankfurt.de.

[2]Present address: Department of Physiology, College of Medicine, Gachon University, 406-799 Incheon, South Korea.

[3]Present address: Institute of Pharmacology, College of Pharmacy, Goethe-University, D-60438 Frankfurt am Main, Germany.

This article contains supporting information online at www.pnas.org/lookup/suppl/doi:10.1073/pnas.1613246113/-/DCSupplemental.

male and female mice (*SI Appendix*, Fig. S1*A*). However, we could not observe any cold allodynia in paclitaxel-treated mice (*SI Appendix*, Fig. S2). We dissected sciatic nerves, DRGs, and the spinal dorsal horn 8 d postinjection. In a directed lipidomic approach, we measured concentrations of oxidized lipid metabolites of the eicosanoid and LA pathway using LC–MS/MS (Fig. 1*G*) and observed increased concentrations of the oxidized LA metabolite 9,10-EpOME in DRGs in both models (Fig. 1 *C* and *D*). There was no difference in 9,10-EpOME concentrations between male and female mice (*SI Appendix*, S1 *B* and *C*). Most interestingly, no other lipids, such as prostanoids or HETEs, were found to be elevated in DRGs in both models (Fig. 1*G* and *SI Appendix*, Table S1). Notably, the concentrations of endocannabinoids and endovanilloids in lumbal DRGs and the dorsal spinal cord showed no difference in vehicle versus high-dose paclitaxel-treated mice 8 d after treatment (*SI Appendix*, Fig. S3 and Table S1*D*). We then investigated expression of the corresponding synthesizing lipid oxygenases of this pathway (COX-2, LOX, CYP2C, and CYP2J isoforms) (14) in DRGs and observed an increase in CYP2J6 transcripts in DRGs of paclitaxel-treated mice in both models, respectively (Fig. 1 *E* and *F*). Accordingly, no other lipid oxygenases showed an increased expression. Reactive oxygen species (ROS) are known mediators that may also contribute to neuropathic pain. Apart from lipid oxygenases (COX, LOX, and CYP), there are other enzymatic sources of ROS (15). To increase the spectrum of potential ROS-producing enzymes in our study (16), we additionally investigated expression of NADPH–oxidases 2 and 4 (NOX-2 and NOX-4) as well as inducible nitric oxide synthase (iNOS) and xanthine–oxidase (XO) in the DRGs of mice 8 d after paclitaxel injection. However, we could not detect any differences in their expression compared with vehicle-treated mice (*SI Appendix*, Fig. S4). Increased concentrations of 9,10-EpOME were already observed 24 h post-paclitaxel injection in DRGs of paclitaxel- but not zymosan-treated mice as controls (*SI Appendix*, Fig. S5 *A–E*). To identify the cellular origin of 9,10-EpOME, both neuronal and glial cultures were stimulated with LA (1 μM). We observed that both neurons and glia synthesize 9,10-EpOME, however the concentrations in neuronal cultures were significantly higher than in glial cultures (*SI Appendix*, Fig. S6*A*). 9,10-EpOME is stable for at least 6 h in any buffer used in this study (*SI Appendix*, Fig. S6 *B* and *C*).

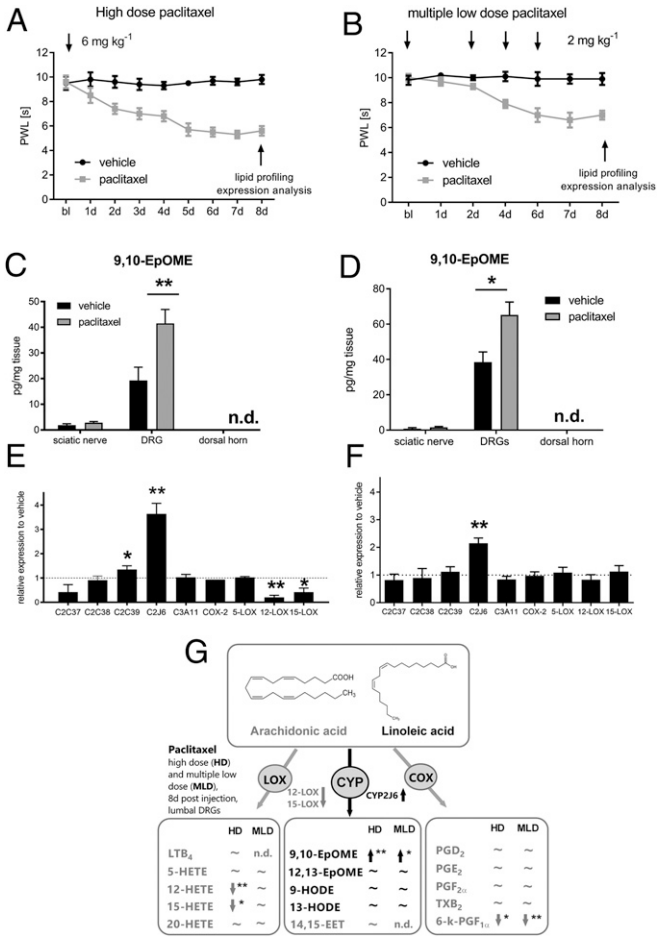

Fig. 1. CYP2J6 is up-regulated in DRGs during PIPN. Time course of the mechanical thresholds of wild-type C57BL/6N mice after injection of (*A*) paclitaxel HD (6 mg·kg^{-1} i.p.; paclitaxel, gray; vehicle, black) and (*B*) MLD (4 × 2 mg·kg^{-1} i.p.; paclitaxel, gray; vehicle, black). Bl, baseline. Data represent means ± SEM of 10 mice per group. Concentrations of 9,10-EpOME in sciatic nerves, DRGs, and the spinal dorsal horn 8 d after i.p. injection of vehicle (black bars) or paclitaxel HD (*C*) or MLD (*D*) (gray bars). *$P < 0.05$, **$P < 0.01$, one-way ANOVA. After 8 d, sciatic nerves, lumbar DRGs, and the spinal dorsal horn were dissected. Expression of murine CYP epoxygenase transcripts 8 d after paclitaxel HD (*E*) or MLD treatment (*F*). Data represent means ± SEM from the DRGs of four mice per group. *$P < 0.05$, **$P < 0.01$, one-way ANOVA; n.d., not determined. (*G*) Scheme of eicosanoid and LA metabolite synthesis in murine DRGs 8 d after paclitaxel HD or MLD treatment as revealed by LC–MS/MS analysis. Data are summarized from *SI Appendix*, Table S1 and represent means ± SEM from three to five mice per group. *$P < 0.05$, **$P < 0.01$, one-way ANOVA. Structures were obtained from lipidmaps.org.

9,10-EpOME Sensitizes TRPV1 but Not TRPA1, TRPV4, or TRPM8 in Sensory Neurons. We hypothesized that 9,10-EpOME may contribute to PIPN and characterized the effects of 9,10-EpOME on primary sensory neurons. A brief exposure to 10 μM 9,10-EpOME caused calcium influx in 10.3% of DRG neurons that could be blocked with the TRPV1 antagonist AMG9810 (1 μM) but not the TRPA1 antagonist HC-030031 (20 μM) (*SI Appendix*, Fig. S7). Next, we set out to test whether 9,10-EpoME can sensitize TRPV1. Indeed, 9,10-EpOME was capable of sensitizing TRPV1-dependent calcium influx (Fig. 2 *A–I*). A concentration response analysis using 9,10-EpOME concentrations from 250 nM to 2 μM revealed a concentration-dependent increase in TRPV1 sensitization. However, mustard oil-dependent TRPA1 responses, GSK1016790A-dependent TRPV4 responses, or menthol-dependent TRPM8 responses could not be sensitized by 9,10-EpOME (1 μM) (Fig. 2*J*).

9,10-EpOME Potentiates TRPV1-Dependent sEPSCs and iCGRP Release from Sensory Neurons via PKA. We examined the effects of 9,10-EpOME in excitatory synaptic transmission in a spinal cord nociceptive circuit. Using patch clamp recordings in spinal cord slices, we measured sEPSCs from outer lamina II (lamina IIo) neurons, as these neurons receive input from TRPV1-expressing primary afferents (17). 9,10-EpOME (1 μM) alone slightly increased the frequency of sEPSCs in IIo neurons. Furthermore, 9,10-EpOME potentiated capsaicin-induced enhancement of sEPSC frequency (Fig. 3 *A* and *B*). Again, our data suggest that 9,10-EpOME also sensitizes TRPV1 in spinal cord central terminals of primary afferents. However, no difference in the amplitude of sEPSCs could be observed with either 9,10-EpOME, capsaicin, or the combination of both substances (Fig. 3*C*), suggesting a possible presynaptic effect of 9,10-EpOME.

Next, sciatic nerves from wild-type BL/6N mice were incubated with 9,10-EpOME alone (1 μM) or together with capsaicin (400 nM), and iCGRP release was measured. We observed a strong increase of immunoreactive CGRP (iCGRP) release with costimulation of capsaicin and 9,10-EpOME (Fig. 3*E*), which could be confirmed in DRG cultures. Because TRPV1 sensitization can be mediated by PKA or PKC (18, 19), we investigated the contribution of these two kinases to EpOME-induced TRPV1 sensitization and observed a reduction of iCGRP release by the PKA inhibitor H89 but not by the

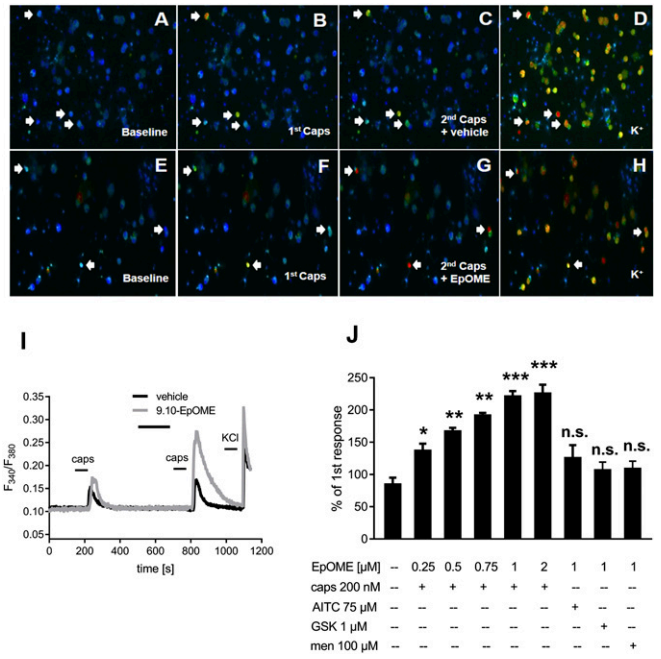

Fig. 2. 9,10-EpOME sensitizes TRPV1 but not TRPA1, TRPV4, or TRPM8 in DRG neurons. (*A–H*) DRG neurons were double-stimulated with capsaicin (caps, 200 nM, 15 s each; *B*, *C*, *F*, and *G*) and preincubated with 9,10-EpOME (1 μM) (*G*) or vehicle (*C*) for 2 min before the second capsaicin stimulation. (*I*) Representative neuronal response to capsaicin with EpOME (gray) or vehicle (black). (*J*) Concentration-dependent TRPV1 sensitization. Concentrations and incubation times for other TRP channel agonists were as follows: AITC (allyisothiocyanate, activates TRPA1, 75 μM, 30 s), GSK1016790A (abbreviated GSK, activates TRPV4, 1 μM, 30 s), and Menthol (abbreviated men, activates TRPM8, 100 μM, 30 s). Data represent the means ± SEM from n = 19–51 neurons; n.s., not significant; $^{*}P < 0.05$, $^{**}P < 0.01$, $^{***}P < 0.001$, one-way ANOVA.

PKC inhibitor GFX (Fig. 3*F*). Similarly, 9,10-EpOME–induced TRPV1 sensitization, as revealed in calcium imaging, could be reduced by preincubation with H89 but not with GFX (*SI Appendix*, Fig. S8), thus pointing toward PKA- but not PKC-mediated TRPV1 sensitization and subsequent iCGRP release by 9,10-EPOME. We also observed a significant increase in cAMP concentrations and increased GTPγS binding after treatment of DRG cultures with 9,10-EpOME.

Injection of 9,10-EpOME Causes Mechanical and Thermal Pain. To determine whether 9,10-EpOME is sufficient to induce pain hypersensitivity in vivo, we injected the lipid in the hind paws of wild-type BL/6N mice and measured the thermal (Fig. 4*A*) and mechanical thresholds (Fig. 4*B*) for 5 h postinjection. These experiments were performed in different groups of animals. 9,10-EpOME caused significant reductions of pain thresholds lasting 1 h (thermal) or 2 h (mechanical) after injection. These effects could not be observed after injection of 9,10-EpOME into the hind paw of TRPV1-deficient mice (Fig. 4 *C* and *D*). To investigate whether TRPV1 is generally involved in paclitaxel-induced mechanical hypersensitivity, we assessed the mechanical thresholds of TRPV1-deficient mice after HD paclitaxel treatment and observed a reduced mechanical hypersensitivity of TRPV1-deficient mice compared with wild-type mice in response to paclitaxel (Fig. 4*E*).

Inhibiting CYP2J2 with Telmisartan Reduces 9,10-EpOME Production as Well as Mechanical and Thermal Hypersensitivity During PIPN. Next, we investigated whether a reduction of CYP2J activity may lead to reduced synthesis of 9,10-EpOME in DRGs. A well-known inhibitor of CYP2J is terfenadine, however this drug causes QT prolongation and was therefore withdrawn from the market (20). Thus, it cannot be repurposed for new indications. To identify other inhibitors of CYP2J, we performed a large compound screen on CYP2J2-expressing supersomes (21–23) with 615 already pharmacologically well-characterized substances and identified, among other substances, the angiotensin-II receptor antagonist telmisartan being a potent inhibitor of CYP2J2 (Fig. 5 *A* and *B* and *SI Appendix*, Figs. S9 and S10 and Table S3).

To exclude that telmisartan has any direct effect on TRP channels, we investigated the effects of telmisartan on TRPV1, TRPA1, and TRPV4 in both calcium-imaging experiments and electrophysiological measurements. Telmisartan (10 μM) did not have any influence on calcium transients or inward currents of TRPV1, TRPA1, or TRPV4 (*SI Appendix*, Fig. S11). Telmisartan and terfenadine, but not their control substances from the same pharmacological group, olmesartan or loratadine (which share the same pharmacological mechanism but do not inhibit CYP2J2), were capable of reducing 9,10-EpOME levels in vitro using transfected HEK-293 cells that were stimulated with LA to trigger EpOME production (*SI Appendix*, Fig. S12). In vivo, the four test substances were injected 8 d after paclitaxel treatment of mice. Two hours after injection of the substances, we isolated sciatic nerves, DRGs, and dorsal spinal cord and sensitively measured various oxidized lipids with LC–MS/MS. We observed a significant reduction of 9,10-EpOME concentrations in DRGs and plasma after treatment with terfenadine or telmisartan but not with olmesartan or loratadine (Fig. 5 *B* and *C* and *SI Appendix*, Table S2).

Next, we tested the substances in behavioral tests during PIPN. We observed that both compounds terfenadine (1 and 2 mg·kg^{-1}) and telmisartan (5 and 10 mg·kg^{-1}) but not their control

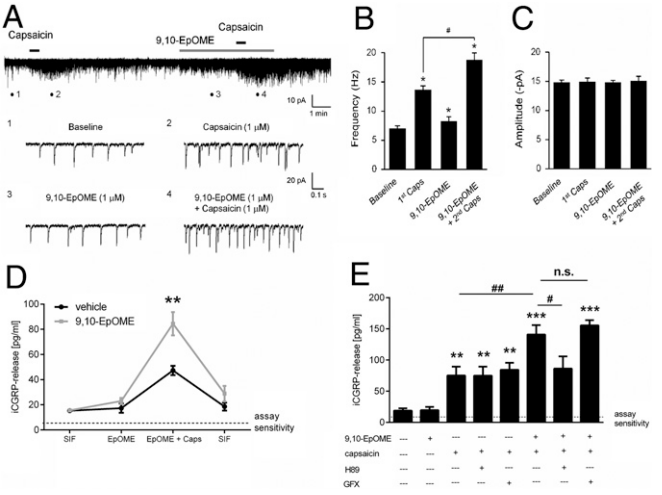

Fig. 3. 9,10-EpOME increases sEPSC frequency in lamina II neurons and sensitizes CGRP release from sciatic nerve and DRGs. (*A*) Traces of sEPSCs in lamina IIo neurons of spinal cord slices. (*Lower*) Traces 1–4 are enlarged and indicate recordings of baseline, first capsaicin (1 μM), 9,10-EpOME (1 μM), and second capsaicin (1 μM) plus 9,10-EpOME, respectively. (*B*) sEPSC frequency and amplitude (*C*) compared with sEPSC baseline, $^{*}P < 0.05$, compared with no treatment baseline; $^{\#}P < 0.05$, compared with the first capsaicin treatment (1 μM); $n = 5$ neurons per group. (*D*) iCGRP release from sciatic nerves stimulated for 5 min with synthetic intestinal fluid (SIF) ± EpOME (1 μM) ± capsaicin (400 nM) or vehicle. Data represent means ± SEM from six individual sciatic nerves. (*E*) Release of iCGRP from DRG cultures stimulated with HBSS ± 9,10-EpOME (1 μM) ± capsaicin (400 nM) ± H89 (PKA inhibitor) (20 μM) or GFX (PKC inhibitor) (1 μM) for 15 min. Data represent means ± SEM of DRG cultures from six to eight mice; n.s., not significant; $^{\#}P < 0.05$, $^{*}P < 0.05$, $^{\#\#}P < 0.05$, $^{**}P < 0.01$, $^{***}P < 0.001$, one-way ANOVA.

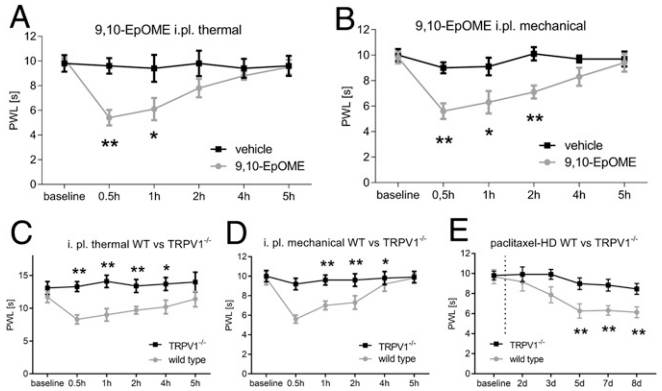

Fig. 4. 9,10-EpOME causes mechanical and thermal pain in vivo. C57BL/6N mice received an intraplantar injection of 10 μL 9,10-EpOME (5 μM, gray) or vehicle [DMSO/saline 0.3% (vol/vol), black]. Thermal (*A*) or mechanical (*B*) thresholds were monitored. Data represent means ± SEM from six to eight mice. Wild-type BL/6N (gray) and TRPV1$^{-/-}$ mice (black) were injected with 10 μL 9,10-EpOME (5 μM) or vehicle [DMSO 0.3% (vol/vol) in saline] intraplantar. Thermal (*C*) or mechanical thresholds (*D*) were monitored. (*E*) Mechanical thresholds of wild-type (gray) versus TRPV1-deficient mice (black) after injection of paclitaxel (HD, 6 mg·kg^{-1} i.p.). Data represent means ± SEM from six mice per group; *$P < 0.05$, **$P < 0.01$, two-way ANOVA with Bonferroni post hoc test.

substances reduced mechanical hypersensitivity in paclitaxel-treated mice (Fig. 6 *A* and *B*). Moreover, we observed that telmisartan alleviated paclitaxel-induced thermal hypersensitivity (Fig. 6*C*). Telmisartan and olmesartan similarly reduced blood pressure in mice, however only telmisartan showed a strong antihyperalgesic effect at 10 mg·kg^{-1}, without affecting motor coordination (*SI Appendix*, Fig. S13). Pretreatment and continuous administration of telmisartan (5 and 10 mg·kg^{-1}) during paclitaxel treatment caused a robust reduction of mechanical hypersensitivity in paclitaxel-treated mice (Fig. 6*C*). A comparison of telmisartan (5 mg·kg^{-1}) and duloxetine (10 mg·kg^{-1}), which is currently the only substance with some clinical efficacy in reducing CIPNP in a clinical trial (24), showed that telmisartan caused a significant reduction of mechanical hypersensitivity. This effect was stronger in telmisartan- than in duloxetine-treated mice at the indicated doses (Fig. 6*D*). Duloxetine treatment had no effect on LA metabolite concentrations in sciatic nerves or DRGs (*SI Appendix*, Fig. S14).

Discussion

In summary, we identified CYP2J6 (human CYP2J2) as a target in PIPN. According to previous reports, CYP2J2 is strongly expressed in human brain tissue (25), which indicates that CYP2J2 is a CYP isoform that is preferably expressed in neuronal tissues. Fittingly, CYP2J4, the rat ortholog of human CYP2J2, is expressed in TRPV1-positive sensory neurons of the trigeminal ganglia (26). Generally, murine CYP2J6 and human CYP2J2 are highly expressed in extrahepatic tissues, such as heart, lung, small intestine, and duodenum (27, 28). This wide distribution of CYP2J isoforms in various tissues indicates that, apart from its drug-metabolizing activity, CYP2J2 has other crucial physiological functions in nonhepatic tissues and points toward a contribution to other pathophysiological pain states.

We showed that enhanced CYP epoxygenase activity is induced by paclitaxel in DRGs, causing synthesis of 9,10-EpOME. Indeed, increased activity of CYP epoxygenases has already been correlated with painful PIPN in patients (29).

Other oxidized linoleic acid metabolites (OLAMs), such as 9- and 13-HODE, have already been shown to be direct TRPV1 agonists and contribute to inflammatory hyperalgesia (30). However, we did not observe any differences in HODE concentrations between paclitaxel- and vehicle-treated mice. Moreover, concentrations of lipids from the LOX and COX-2 pathway, which have previously been identified as modulators of TRP channels in various pain models (31–33), were not increased during PIPN. Previous reports suggest a role for CYP and LOX metabolites in NGF-dependent thermal and mechanical nociception, and inhibition of CYP and LOX enzymes with the unspecific inhibitor NDGA may reduce NGF-dependent hypersensitivity (34). However, in our study, the concentrations of LOX products, such as HETEs, were either not changed or even decreased in DRGs and the spinal cord during PIPN. These results imply an entirely different mechanism of oxidized lipid synthesis during PIPN, compared with inflammatory pain or NGF-dependent hypersensitivity in DRGs and the spinal cord, and point out the significance of the CYP pathway during PIPN.

Chemotherapy-induced neuropathic pain and subsequent sensory dysfunctions still remain the most severe side effects of cytostatics (35). Especially during paclitaxel treatment, an early acute pain syndrome can be observed that seems to be mediated by sensitization of nociceptive neurons (36). However, there is no information available on endogenous mediators that may contribute to this pathophysiological state. According to our data, 9,10-EpOME–dependent TRPV1 sensitization and increased activity of nociceptive neurons may thus contribute to paclitaxel acute pain syndrome.

Recently, promising results were reported with an angiotensin (AT2) antagonist in a phase 2 study with patients suffering from postherpetic neuralgia (37). However, telmisartan targets a different angiotensin receptor (AT1), and control experiments with olmesartan suggest that this mechanism is not responsible for the antihyperalgesic effects of telmisartan.

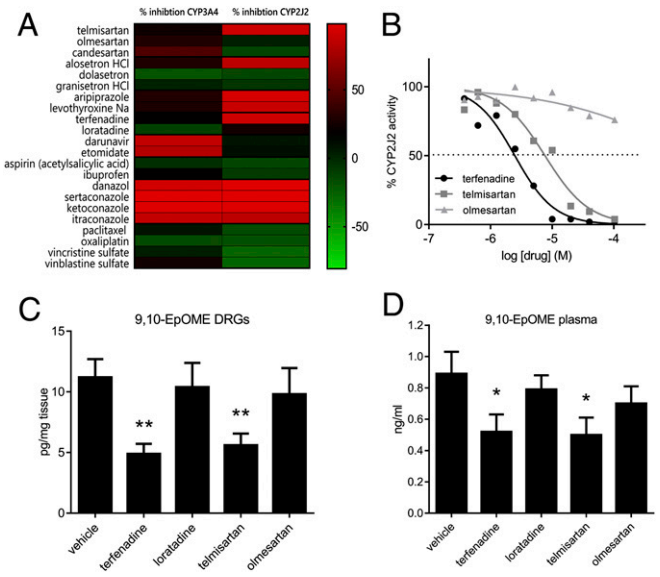

Fig. 5. Inhibition of CYP2J6/2 by telmisartan reduces lipid concentrations in vitro and in vivo and reduces paclitaxel-induced CIPNP in vivo. (*A*) Heat map depicting a selection of the 615 tested substances from the drug repurposing screen. Inhibition of CYP3A4 (*Left*) was tested as the control. For each substance and each CYP protein, the assay was performed in technical duplicates. The full list of 615 drugs is shown in *SI Appendix*, Table S3. (*B*) Dose–response analysis of terfenadine (black), telmisartan (dark gray), and olmesartan (light gray) (each 300 nM to 40 μM) on CYP2J2 activity, measured in triplicates on a 96-well plate. Concentrations of 9,10-EpOME in lumbar DRGs (*C*) and plasma (*D*) of wild-type mice that had received paclitaxel (6 mg·kg^{-1}) 8 d before and were then treated with either 1 mg·kg^{-1} terfenadine, 1 mg·kg^{-1} loratadine, 5 mg·kg^{-1} telmisartan, or 5 mg·kg^{-1} olmesartan for 2 h, summarized from *SI Appendix*, Table S2. Data are shown as means from six mice per group. *$P < 0.05$, **$P < 0.05$, one-way ANOVA.

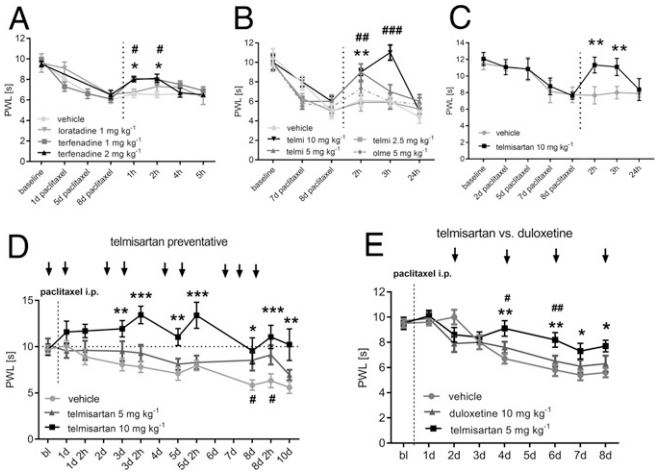

Fig. 6. Inhibition of CYP2J6/2 by telmisartan reverses paclitaxel-induced mechanical and thermal hypersensitivity in vivo. (*A*) Mechanical thresholds of mice treated with paclitaxel for 8 d (6 mg·kg^{-1}) receiving an injection of terfenadine (*1 or $^{\#}$2 mg·kg^{-1}, black and dark gray), loratadine (1 mg·kg^{-1}, gray), or vehicle [DMSO 2.5% or 5% (vol/vol), light gray]. (*B*) Mechanical thresholds of mice treated with telmisartan (telmi, 2.5, *5, or $^{\#}$10 mg·kg^{-1}, black to light gray), olmesartan (olme, 5 mg·kg^{-1}, dashed), or vehicle 8 d after paclitaxel injection (6 mg·kg^{-1}). (*C*) Thermal thresholds of wild-type mice that received a paclitaxel injection (6 mg·kg^{-1}) and were treated with telmisartan (10 mg·kg^{-1}, black) or vehicle (gray) 8 d after paclitaxel injection. (*D*) Mechanical thresholds of wild-type mice that received a paclitaxel injection (6 mg·kg^{-1}) and were treated with telmisartan ($^{\#}$5 or *10 mg·kg^{-1}) or vehicle every day for 8 d. (*E*) Mechanical thresholds of wild-type mice after paclitaxel injection (6 mg·kg^{-1}) treated with telmisartan (5 mg·kg^{-1}), duloxetine (10 mg·kg^{-1}), or vehicle every second day for 8 d. $^{\#}$Telmisartan vs. duloxetine. All substances were applied i.p. Data represent means ± SEM from six to nine mice per group. *$P < 0.05$, $^{\#}P < 0.05$, **$P < 0.05$, $^{\#\#}P < 0.05$, ***$P < 0.001$, $^{\#\#\#}P < 0.01$, two-way ANOVA with Bonferroni post hoc test.

Currently, there is a strong unmet medical need for CIPNP therapeutics. Paclitaxel is still the preferred first-line treatment for metastatic breast cancer (12, 38). Treatment of patients with antioxidants or neuroprotective substances, such as amifostine or glutathione, failed to ameliorate CIPNP in large randomized and placebo-controlled clinical trials, and a recent Cochrane review concludes that there is currently no evidence for functional CIPNP therapy with these substances (39). Moreover, antioxidants may interfere with the antineoplastic effects of cytostatics. Recently, it was reported that treatment with *N*-acetyl cysteine (NAC) and vitamin E increased lung tumor cell proliferation and tumor growth in mice by reducing DNA damage (40). In this regard, CYP2J2 inhibitors may be superior over using antioxidants, as CYP2J2 inhibitors have been reported to even reduce cancer growth in vitro and in vivo by activating caspase-3, Bax, and Bcl-2 and by reducing tumor cell migration and adherence (41). Thus, CYP2J2 inhibitors may have a dual role in reducing both cancer growth and taxane-induced CIPNP.

Methods

Animals and Ethical Approval. All procedures performed in studies involving animals were in accordance with the ethical standards of the *Guide for the Care and Use of Laboratory Animals* of the National Institutes of Health (42) and were approved by the local Ethics Committees for Animal Research (Darmstadt) under permit no. F95/47.

For all behavioral experiments, we used only 6–12-wk-old C57BL/6N male and female mice purchased from commercial breeding companies (Charles River and Janvier). To compare mechanical thresholds, we used age- and sex-matched littermates as control.

A breeding pair of TRPV1-deficient mice were purchased from Jackson, and the animals were bred in the laboratory animal facility of the University Hospital of Goethe-University.

Paclitaxel Model of Chemotherapy-Induced Neuropathic Pain. Paclitaxel was solved in Cremophor EL/Ethanol 1:1 and diluted in saline. The dose for i.p. injection was set to 6 mg·kg^{-1} for the HD model or 2 mg·kg^{-1} for the multiple LDM, as described previously (2, 13).

Behavioral Tests. Behavioral tests were performed as described previously (43). Briefly, for the assessment of the mechanical thresholds, the steel rod was pushed against the midplantar hind paw with linear ascending force (0–5 g over 10 s, increasing 0.5 g/s) until a fast withdrawal response occurred. For determination of thermal thresholds, the midplantar region of the paws was stimulated with a radiant heat device, consisting of a high-intensity projector lamp, until withdrawal occurred.

Blood Pressure Measurement. For blood pressure measurements, mice were habituated to the IITC Life Science tail cuff apparatus (IITC Life Sciences) for at least 5 d before actual measurements were performed. Mice were placed in the restrainer in the apparatus with the chamber temperature set to 34 °C. Two hours after treatment with telmisartan (10 mg·kg^{-1} i.p.), olmesartan (5 mg·kg^{-1} i.p.), or vehicle [5% (vol/vol) DMSO in 0.9% NaCl i.p.], systolic blood pressure (SBP) was measured. Data points were excluded when the signal was not readable, tail pulses were not detected, or the mouse was moving during measurement. The average measurement per mouse over 2–3 d was analyzed to calculate the SBP for the mouse, for that particular treatment.

Primary DRG Cultures. Primary DRGs were cultured as described previously (43, 44). Briefly, murine DRGs were dissected from spinal segments and directly transferred to ice-cold HBSS with $CaCl_2$ and $MgCl_2$, incubated with collagenase/dispase (500 U/mL Collagenase; 2.5 U/mL Dispase), washed twice with neurobasal medium containing 10% (vol/vol) FCS, and incubated for 10 min with 0.05% trypsin (Invitrogen). Finally, the neurons were plated on poly-L-lysine– (Sigma) coated glass coverslips and incubated with neurobasal medium containing L-glutamine (2 mM) penicillin (100 U/mL), streptomycin (100 μg/mL), and B-27 and gentamicin (50 μg/mL) over night until assessment by calcium imaging.

Calcium-Imaging Experiments. Calcium-imaging experiments were performed using DRG neurons 24–48 h after preparation. Cells were loaded with 5 μM Fura-2-AM-ester (Biotium) and incubated for 30–60 min at 37 °C. Then, the cells were washed with standard external solution [containing in mM: NaCl (145), $CaCl_2$ (1.25), $MgCl_2$ (1), KCl (5), D-glucose (10), and Hepes (10), adjusted to pH 7.3]. Baseline measurements were performed in external solution at a flow rate of 1–2 mL/min. Calcium-free solutions were generated by removal of $CaCl_2$ and addition of EGTA (2 mM) and osmotically controlled by increasing NaCl concentrations to 150 mM. Stock solutions of HC-030031, AITC, menthol, GSK1016790A (Sigma), AMG9810, H89-dihydrochloride, 8-bromo-cAMP, GF 109203X (all from Tocris), and NGF (Merck Millipore) were diluted in external solution to their final concentrations.

Patch-Clamp Recordings from Spinal Cord Slices. Patch-clamp recordings from spinal cord slices were performed as described previously (17). Briefly, a portion of the lumbar spinal cord (L4–L5) was removed from mice (CD1, 5–7 wk old; Charles River Laboratories) under urethane anesthesia (1.5–2.0 g/kg, i.p.) and kept in preoxygenated ice-cold Krebs solution. Transverse slices (400–600 μm) were cut on a vibrating microslicer. After establishing the whole-cell configuration, neurons were held at their holding potentials at –70 mV for recording sEPSCs.

Quantitative Real-Time PCR. Lumbal DRGs were dissected from mice at indicated time points, and RNA was extracted using the *mir*Vana miRNA Isolation Kit (Ambion, Life Technologies). Reverse transcription and real-time PCR were performed using the TaqMan system (Life Technologies) and evaluated with the ΔΔC(T) method as described previously (45). For 5-LOX, 12-LOX, 15-LOX, COX-2, NOX-2, NOX-4, iNOS, and XO, assay primers for the TaqMan system (ThermoFisher) were used. The oligonucleotides that were used for expression analysis of CYP epoxygenases are depicted in *SI Appendix*, Table S4.

Determination of Lipidomic Profiles by LC–MS/MS. Stock solutions with 2,500 ng/mL of the analytes 9,10-EpOME, 12,13-EpOME, 9,10-Dihydroxyoctadecenoic acid (DiHOME), 12,13-DiHOME, 5,6 EET, 8,9 EET, 11,12 EET, 14,15 EET, Leukotriene B_4 (LTB_4), 5-S-HETE, 12-S-HETE, and 15-S-HETE and the internal standards 9,10-EpOME-d4, 12,13-EpOME-d4, 9,10-DiHOME-d4, 12,13-DiHOME-d4, 5,6 EET-d11, 8,9 EET-d11, 11,12 EET-d8, 14,15 EET-d8, LTB_4-d4, 5-S-HETE-d4, 12-S-HETE-d4, and 15-S-HETE-d4 were prepared in methanol. Working standards were obtained by further dilution with a concentration range of 0.1–250 ng/mL for all analytes. For prostanoids, stock solutions with 50,000 ng/mL of all analytes (PGE_2, PGD_2,

6-keto-$PGF_{1\alpha}$, TXB_2, and $PGF_{2\alpha}$) and the internal standards (PGE_2-d4, PGD_2-d4, 6-keto-$PGF_{1\alpha}$-d4, TXB_2-d4, and $PGF_{2\alpha}$-d4) were prepared in methanol. Working standards were obtained by further dilution with a concentration range of 0.1–1,250 ng/mL for PGE_2, PGD_2, 6-keto-$PGF_{1\alpha}$, and TXB_2 and 0.4–5,000 ng/mL for $PGF_{2\alpha}$. Sample pretreatment was performed using liquid–liquid extraction. Therefore, homogenated tissue was extracted twice with 600 μL of ethyl acetate. The combined organic phases were removed at a temperature of 45 °C under a gentle stream of nitrogen. The residues were reconstituted with 50 μL of methanol/water/butylated hydroxytoluene (50:50:10^{-3}, vol/vol/v) (EETs and leukotrienes) or 50 μL of acetonitrile/water/formic acid (20:80:0.0025, vol/vol/v) (prostanoids), centrifuged for 2 min at 10,000 × *g*, and transferred to glass vials before analysis. Sample extraction, chromatographic separation, and lipid quantification were performed as described previously (46). For details, see *SI Appendix*.

[^{35}S]GTPγS Binding Assays. To measure activation of a putative G protein-coupled receptor, GTPγS binding assays were performed as described previously (47) using 1 μM 9,10-EpOME (Cayman) and fresh [^{35}S]GTPγS (1,250 Ci/mmol; Perkin–Elmer).

Measurement of iCGRP, cAMP, and CYP Epoxygenase Activity. CGRP measurements were performed as described previously (48) using a CGRP enzyme immune assay kit (SpiBio, Bertin Pharma). Also, cAMP measurements were performed using a luminescence-based P450-Glo Assay by Promega using Forskolin (Sigma) and Cicaprost (Cayman) as controls.

CYP2J2 and CYP3A4 activity assays were performed with two different kits according to the manufacturers' instructions: the luminescence-based P450-Glo assay by Promega and the fluorescence-based Vivid CYP450 Screening Kit from Life Technologies. As an enzymatic source, CYP2J2 and CYP3A4 supersomes by Corning were used. The positive controls were terfenadine (CYP2J2) and ketoconazole (CYP3A4). The substance screen was performed at the Fraunhofer Screeningport (www.screeningport.com). For transfection of HEK cells, pCMV-AC-GFP plasmids containing genes for CYP2J6 or CYP3A11 were purchased from Origene and LA (1 μM) (Sigma) was used as a substrate for CYP2J2.

Data Analysis and Statistics. All data are presented as means ± SEM. To determine statistically significant differences in all behavioral experiments, two-way analysis of variance (ANOVA) for repeated measures was used followed by post hoc Bonferroni correction using GraphPad Prism. For in vitro experiments comparing only two groups, one-way ANOVA was carried out, and $P < 0.05$ was considered statistically significant.

ACKNOWLEDGMENTS. The support of the Landesoffensive zur Entwicklung Wissenschaftlich-ökonomischer Exzellenz (LOEWE)-Center Translational Medicine and Pharmacology is gratefully acknowledged. This work was supported by DFG (German Research Association) Grants SFB1039 TPA08, TPA09, and TPZ01; DFG Excellence Cluster 147 (ECCPS); and NIH Grant R01NS67686 (to R.-R.J.).

1. Nassini R, et al. (2011) Oxaliplatin elicits mechanical and cold allodynia in rodents via TRPA1 receptor stimulation. *Pain* 152(7):1621–1631.
2. Alessandri-Haber N, Dina OA, Joseph EK, Reichling DB, Levine JD (2008) Interaction of transient receptor potential vanilloid 4, integrin, and SRC tyrosine kinase in mechanical hyperalgesia. *J Neurosci* 28(5):1046–1057.
3. Hara T, et al. (2013) Effect of paclitaxel on transient receptor potential vanilloid 1 in rat dorsal root ganglion. *Pain* 154(6):882–889.
4. Materazzi S, et al. (2012) TRPA1 and TRPV4 mediate paclitaxel-induced peripheral neuropathy in mice via a glutathione-sensitive mechanism. *Pflugers Arch* 463(4):561–569.
5. Li Y, et al. (2015) The cancer chemotherapeutic paclitaxel increases human and rodent sensory neuron responses to TRPV1 by activation of TLR4. *J Neurosci* 35(39):13487–13500.
6. Talme T, Liu Z, Sundqvist KG (2008) The neuropeptide calcitonin gene-related peptide (CGRP) stimulates T cell migration into collagen matrices. *J Neuroimmunol* 196(1-2):60–66.
7. Chiu IM, von Hehn CA, Woolf CJ (2012) Neurogenic inflammation and the peripheral nervous system in host defense and immunopathology. *Nat Neurosci* 15(8):1063–1067.
8. Chen Y, Yang C, Wang ZJ (2011) Proteinase-activated receptor 2 sensitizes transient receptor potential vanilloid 1, transient receptor potential vanilloid 4, and transient receptor potential ankyrin 1 in paclitaxel-induced neuropathic pain. *Neuroscience* 193:440–451.
9. Dai D, et al. (2001) Polymorphisms in human CYP2C8 decrease metabolism of the anticancer drug paclitaxel and arachidonic acid. *Pharmacogenetics* 11(7):597–607.
10. Spector AA, Norris AW (2007) Action of epoxyeicosatrienoic acids on cellular function. *Am J Physiol Cell Physiol* 292(3):C996–C1012.
11. Wen H, et al. (2012) 20-hydroxyeicosatetraenoic acid (20-HETE) is a novel activator of TRPV1. *J Biol Chem* 287(17):13868–13876.
12. Gligorov J, Richard S (2015) Breast cancer: Weekly paclitaxel–Still preferred first-line taxane for mBC. *Nat Rev Clin Oncol* 12(9):508–509.
13. Nieto FR, et al. (2008) Tetrodotoxin inhibits the development and expression of neuropathic pain induced by paclitaxel in mice. *Pain* 137(3):520–531.
14. Imig JD, Hammock BD (2009) Soluble epoxide hydrolase as a therapeutic target for cardiovascular diseases. *Nat Rev Drug Discov* 8(10):794–805.
15. Kim HK, et al. (2004) Reactive oxygen species (ROS) play an important role in a rat model of neuropathic pain. *Pain* 111(1-2):116–124.
16. Holmström KM, Finkel T (2014) Cellular mechanisms and physiological consequences of redox-dependent signalling. *Nat Rev Mol Cell Biol* 15(6):411–421.
17. Park CK, et al. (2011) Resolving TRPV1- and TNF-α-mediated spinal cord synaptic plasticity and inflammatory pain with neuroprotectin D1. *J Neurosci* 31(42):15072–15085.
18. Schnizler K, et al. (2008) Protein kinase A anchoring via AKAP150 is essential for TRPV1 modulation by forskolin and prostaglandin E2 in mouse sensory neurons. *J Neurosci* 28(19):4904–4917.
19. Bhave G, et al. (2003) Protein kinase C phosphorylation sensitizes but does not activate the capsaicin receptor transient receptor potential vanilloid 1 (TRPV1). *Proc Natl Acad Sci USA* 100(21):12480–12485.
20. Roden DM (2004) Drug-induced prolongation of the QT interval. *N Engl J Med* 350(10):1013–1022.
21. Parikh S, et al. (2003) CYP2J2 and CYP4F12 are active for the metabolism of non-sedating antihistamines: Terfenadine and astemizole. *Drug Metab Rev* 35:190–191.
22. Eagling VA, Tjia JF, Back DJ (1998) Differential selectivity of cytochrome P450 inhibitors against probe substrates in human and rat liver microsomes. *Br J Clin Pharmacol* 45(2):107–114.
23. Eagling VA, Wiltshire H, Whitcombe IW, Back DJ (2002) CYP3A4-mediated hepatic metabolism of the HIV-1 protease inhibitor saquinavir in vitro. *Xenobiotica* 32(1):1–17.
24. Smith EM, et al.; Alliance for Clinical Trials in Oncology (2013) Effect of duloxetine on pain, function, and quality of life among patients with chemotherapy-induced painful peripheral neuropathy: A randomized clinical trial. *JAMA* 309(13):1359–1367.
25. Dutheil F, et al. (2009) Xenobiotic-metabolizing enzymes and transporters in the normal human brain: Regional and cellular mapping as a basis for putative roles in cerebral function. *Drug Metab Dispos* 37(7):1528–1538.
26. Ruparel S, et al. (2012) Plasticity of cytochrome P450 isozyme expression in rat trigeminal ganglia neurons during inflammation. *Pain* 153(10):2031–2039.
27. Graves JP, et al. (2015) Quantitative polymerase chain reaction analysis of the mouse Cyp2j subfamily: Tissue distribution and regulation. *Drug Metab Dispos* 43(8):1169–1180.
28. Bièche I, et al. (2007) Reverse transcriptase-PCR quantification of mRNA levels from cytochrome (CYP)1, CYP2 and CYP3 families in 22 different human tissues. *Pharmacogenet Genomics* 17(9):731–742.
29. Hertz DL, et al. (2013) CYP2C8*3 increases risk of neuropathy in breast cancer patients treated with paclitaxel. *Ann Oncol* 24(6):1472–1478.
30. Patwardhan AM, et al. (2010) Heat generates oxidized linoleic acid metabolites that activate TRPV1 and produce pain in rodents. *J Clin Invest* 120(5):1617–1626.
31. Gregus AM, et al. (2012) Spinal 12-lipoxygenase-derived hepoxilin A3 contributes to inflammatory hyperalgesia via activation of TRPV1 and TRPA1 receptors. *Proc Natl Acad Sci USA* 109(17):6721–6726.
32. Ricciotti E, FitzGerald GA (2011) Prostaglandins and inflammation. *Arterioscler Thromb Vasc Biol* 31(5):986–1000.
33. Hwang SW, et al. (2000) Direct activation of capsaicin receptors by products of lipoxygenases: Endogenous capsaicin-like substances. *Proc Natl Acad Sci USA* 97(11):6155–6160.
34. Eskander MA, et al. (2015) Persistent nociception triggered by nerve growth factor (NGF) is mediated by TRPV1 and oxidative mechanisms. *J Neurosci* 35(22):8593–8603.
35. Pachman DR, Barton DL, Watson JC, Loprinzi CL (2011) Chemotherapy-induced peripheral neuropathy: Prevention and treatment. *Clin Pharmacol Ther* 90(3):377–387.
36. Loprinzi CL, et al. (2007) The Paclitaxel acute pain syndrome: Sensitization of nociceptors as the putative mechanism. *Cancer J* 13(6):399–403.
37. Rice AS, et al.; EMA401-003 study group (2014) EMA401, an orally administered highly selective angiotensin II type 2 receptor antagonist, as a novel treatment for postherpetic neuralgia: A randomised, double-blind, placebo-controlled phase 2 clinical trial. *Lancet* 383(9929):1637–1647.
38. Rugo HS, et al. (2015) Randomized phase III trial of paclitaxel once per week compared with nanoparticle albumin-bound Nab-paclitaxel once per week or ixabepilone with bevacizumab as first-line chemotherapy for locally recurrent or metastatic breast cancer: CALGB 40502/NCCTG N063H (Alliance). *J Clin Oncol* 33(21):2361–2369.
39. Albers JW, Chaudhry V, Cavaletti G, Donehower RC (2011) Interventions for preventing neuropathy caused by cisplatin and related compounds. *Cochrane Database Syst Rev* (2):CD005228.
40. Sayin VI, et al. (2014) Antioxidants accelerate lung cancer progression in mice. *Sci Transl Med* 6(221):221ra15.
41. Chen C, et al. (2009) Selective inhibitors of CYP2J2 related to terfenadine exhibit strong activity against human cancers in vitro and in vivo. *J Pharmacol Exp Ther* 329(3):908–918.
42. National Research Council (2011) *Guide for the Care and Use of Laboratory Animals* (The National Academies Press, Washington, DC), 8th Ed.
43. Sisignano M, et al. (2012) 5,6-EET is released upon neuronal activity and induces mechanical pain hypersensitivity via TRPA1 on central afferent terminals. *J Neurosci* 32(18):6364–6372.
44. Lu R, et al. (2015) Slack channels expressed in sensory neurons control neuropathic pain in mice. *J Neurosci* 35(3):1125–1135.
45. Livak KJ, Schmittgen TD (2001) Analysis of relative gene expression data using real-time quantitative PCR and the 2(-Delta Delta C(T)) method. *Methods* 25(4):402–408.
46. Sisignano M, et al. (2013) Synthesis of lipid mediators during UVB-induced inflammatory hyperalgesia in rats and mice. *PLoS One* 8(12):e81228.
47. Oertel BG, et al. (2009) A common human micro-opioid receptor genetic variant diminishes the receptor signaling efficacy in brain regions processing the sensory information of pain. *J Biol Chem* 284(10):6530–6535.
48. Brenneis C, et al. (2011) Soluble epoxide hydrolase limits mechanical hyperalgesia during inflammation. *Mol Pain* 7:78.